

Geophysical Research Letters

RESEARCH LETTER

10.1029/2020GL088976

Key Points:

- Novel statistical EMIC diffusion coefficients are determined using simultaneous observations of the individual plasma and wave parameters
- The new diffusion coefficients show that EMIC waves diffuse electrons over a wide range of energies and pitch angles
- When included into 3-D radiation belt simulations, the new diffusion coefficients significantly improve agreement with observations

Correspondence to:

J. P. J. Ross,
johros@bas.ac.uk

Citation:

Ross, J. P. J., Glauert, S. A., Horne, R. B., Watt, C. E., Meredith, N. P., & Woodfield, E. E. (2020). A new approach to constructing models of electron diffusion by EMIC waves in the radiation belts. *Geophysical Research Letters*, 47, e2020GL088976. <https://doi.org/10.1029/2020GL088976>

Received 29 MAY 2020

Accepted 3 SEP 2020

Accepted article online 7 OCT 2020

A New Approach to Constructing Models of Electron Diffusion by EMIC Waves in the Radiation Belts

J. P. J. Ross¹ , S. A. Glauert¹ , R. B. Horne¹ , C. E. Watt² , N. P. Meredith¹ , and E. E. Woodfield¹ 

¹British Antarctic Survey, Natural Environment Research Council, Cambridge, UK, ²Department of Mathematics, Physics and Electrical Engineering, Northumbria University, Newcastle-upon-Tyne, UK

Abstract Electromagnetic ion cyclotron (EMIC) waves play an important role in relativistic electron losses in the radiation belts through diffusion via resonant wave-particle interactions. We present a new approach for calculating bounce and drift-averaged EMIC electron diffusion coefficients. We calculate bounce-averaged diffusion coefficients, using quasi-linear theory, for each individual Combined Release and Radiation Effects Satellite (CRRES) EMIC wave observation using fitted wave properties, the plasma density and the background magnetic field. These calculations are then combined into bounce-averaged diffusion coefficients. The resulting coefficients therefore capture the combined effects of individual spectra and plasma properties as opposed to previous approaches that use average spectral and plasma properties, resulting in diffusion over a wider range of energies and pitch angles. These calculations, and their role in radiation belt simulations, are then compared against existing diffusion models. The new diffusion coefficients are found to significantly improve the agreement between the calculated decay of relativistic electrons and Van Allen Probes data.

Plain Language Summary In recent years there have been an increasing number of satellites operating in or traversing the Earth's radiation belts. These belts are composed of charged particles that are largely confined by the Earth's magnetic field, although waves can accelerate and scatter these particles. In the outer belt, electrons can be accelerated up to relativistic energies and pose a threat to satellites. Diffusion-based models are used to simulate the electron population, incorporating the statistical effects of waves on the electrons. Electromagnetic ion cyclotron waves are of particular importance for the relativistic population, effectively scattering them into the atmosphere and removing them from the belts. Previous models of this interaction are based on average plasma and wave observations; however, these do not well represent the range of interactions possible. Here we take a new approach, considering each observation individually to determine their statistical effect. When included into diffusion models, this new approach significantly improves the modeling of the relativistic electron population.

1. Introduction

The electrons that make up the outer electron radiation belt exist over a wide range of energies, extending up to well over 10 MeV, where curvature and gradient drift dominates and they complete closed paths around the Earth. Electrons can be rapidly accelerated up to relativistic energies during geomagnetic storms through a combination of wave-particle interactions with whistler mode chorus waves (Horne, Thorne, Glauert, et al., 2005; Horne, Thorne, Shprits, et al., 2005), shocks (Blake et al., 1992), and radial transport (Schulz & Lanzerotti, 1974). Relativistic electron fluxes can be increased by several orders of magnitude (Baker et al., 1994; Reeves et al., 2003) on the timescale of hours to days and can pose a risk to satellite instrumentation (Wrenn et al., 2002). These fluxes then decay on timescales of 5–10 days (Claudepierre et al., 2020; Meredith et al., 2006), and it is believed that their removal is strongly influenced by pitch angle diffusion by electromagnetic ion cyclotron (EMIC) waves (Albert, 2003; Horne & Thorne, 1998). Coincident observations of EMIC waves and relativistic electron precipitation support the idea that EMIC waves are influential at scattering MeV electrons (Miyoshi et al., 2008; Rodger et al., 2008; Usanova et al., 2014; Yuan et al., 2018). The effects of EMIC waves can also be seen in the narrowing of ultrarelativistic electron pitch angle distributions (Kersten et al., 2014; Shprits et al., 2016; Usanova et al., 2014) and deepening of local minima in phase space density (Shprits et al., 2017).

©2020. The Authors.

This is an open access article under the terms of the Creative Commons Attribution License, which permits use, distribution and reproduction in any medium, provided the original work is properly cited.

Electron resonance with EMIC waves, and hence diffusion, is sensitive to both the wave spectrum and the plasma properties (Meredith et al., 2003; Summers et al., 2007). For instance, increasing the electron density decreases the minimum resonant energy and allows diffusion at larger pitch angles, providing a mechanism by which near-equatorial mirroring electrons can be removed. Similarly, for wave frequencies that approach the respective ion cyclotron frequency from below, the minimum resonant energy can be reduced down to ~ 400 keV (Ukhorskiy et al., 2010). In fact, studies using helium band EMIC waves with Gaussian spectra with central frequencies of $0.9f_{cHe}$, where f_{cHe} is the helium ion gyrofrequency, have been found to improve the agreement between radiation belt models of the $\gtrsim 1$ MeV electron flux and observations (Drozdov et al., 2017; Ma et al., 2015). It is unclear, however, whether such a spectrum is representative of the EMIC waves in the radiation belts given that mean wave frequency to gyrofrequency ratios observations are on average substantially below these adopted values. More specifically, are EMIC waves with characteristics in the tails of the wave frequency and plasma density distributions sufficiently efficient at diffusing near-equatorially mirroring MeV energy electrons to provide observed levels of electron losses?

In this paper we present a new approach for calculating the average quasi-linear diffusion coefficients for the diffusion of relativistic electrons by averaging over observation-specific bounce-averaged diffusion coefficients. We begin by illustrating the variability of EMIC observations in section 2. In section 3 we then present an alternative method of calculating statistical bounce-averaged EMIC diffusion coefficients by performing bounce-averaged diffusion calculations for each EMIC wave observation before averaging over the observations. These new diffusion coefficients are then compared to existing models using average wave and plasma properties. In section 4, the new coefficients are included into 3-D Fokker-Plank based radiation belt simulations to assess the effect of the new diffusion coefficients on the relativistic electron population.

2. EMIC Wave Spectra

For this study, we use data from the Combined Release and Radiation Effects Satellite (CRRES) (Johnson & Kierein, 1992). The magnetic field was measured by the 16 Hz fluxgate magnetometer (Singer et al., 1992) and provides the ambient magnetic field from which we determine the gyrofrequencies. Additionally, the field measurements are fast Fourier transformed using 1,600 points with a 400 point step to obtain wave spectra extending from 0 to 8 Hz in steps of 10 mHz at a 25.6 s resolution. Each spectral profile is analyzed, and two Gaussian functions are fitted, one for the hydrogen band and the other for the helium band (Meredith et al., 2014). Noise spikes and bands that do not have Gaussian profiles are omitted. For each Gaussian profile, we have the peak power spectral density, PSD_m , the corresponding peak frequency f_m , and width, f_w , defined by

$$PSD = PSD_m e^{-\left(\frac{f-f_m}{f_w}\right)^2}. \quad (1)$$

The plasma densities are derived from the plasma wave spectra measured by the Plasma Wave Experiment (Anderson et al., 1992) as described in Meredith et al. (2002). We store the central frequency of the fitted Gaussian f_m/f_{cHe} , the Gaussian width f_w/f_{cHe} and the wave intensity B_w^2 , and the corresponding electron plasma frequency to electron gyrofrequency ratio, f_{pe}/f_{ce} , together with L^* , the magnetic latitude λ_m , and the associated activity indices (AE , K_p , Dst , and solar wind pressure, P_{dyn}). Here f_{cHe} is the helium gyrofrequency. The geomagnetic coordinates are calculated using the ONERA-DESP library and the International Geomagnetic Reference Field at the middle of the corresponding year combined with the Olson-Pfizer quiet time model (Olson & Pfizer, 1977).

Key parameters in determining wave-particle interactions include the wave intensity, $B_w^2(nT^2)$, the proton gyrofrequency, f_{cp} , and the plasma density. In Figures 1a and 1b we show scatter plots of $B_w^2(nT^2)$ against the determined f_{pe}/f_{ce} for H^+ and He^+ EMIC bands, respectively. For comparison, the constant value of $f_{pe}/f_{ce} = 10$ that was used in Kersten et al. (2014) (henceforth Kersten2014) is overlaid. To aid with interpretation we over plot the survival function of f_{pe}/f_{ce} , where the survival function S of parameter x with probability density function, $f(x)$, is defined as

$$S(X) = \int_X^\infty f(s)ds. \quad (2)$$

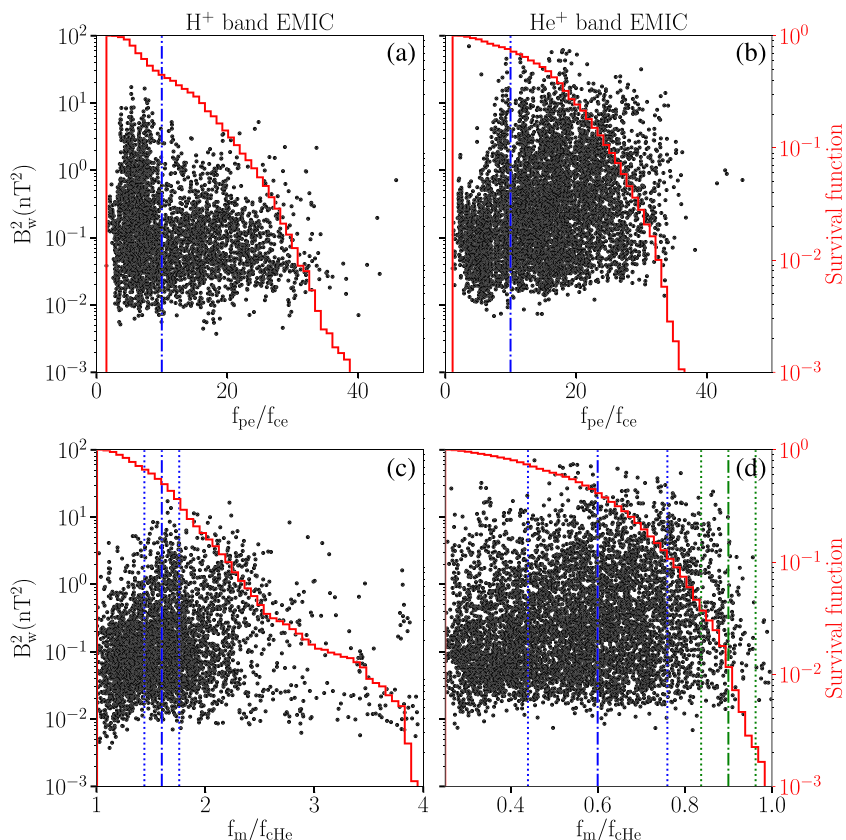


Figure 1. The observed hydrogen (a) and helium (b) band EMIC wave intensities against f_{pe}/f_{ce} . The dash-dotted blue lines indicate f_{pe}/f_{ce} used by Kersten et al. (2014) in their diffusion coefficient calculations. Subplots (c) and (d) show the same as (a) and (b) but for f_m/f_{cHe} . The dash-dotted blue and green lines indicate f_m/f_{cHe} used by Kersten et al. (2014) and Ma et al. (2015), respectively. The corresponding upper and lower-frequency cutoffs are indicated by the dotted lines of the same color. On each of the subplots the solid red line shows the survival function of the frequency ratio shown on the x axes (not weighted by wave power).

Intuitively, for a given X , $S(X)$ can be interpreted as the probability that x exceeds X . The survival function is one minus the cumulative distribution function. Strong wave power is observed over a wide range of f_{pe}/f_{ce} , with $f_{pe}/f_{ce} > 20 \gtrsim 10\%$ of the time and reaches ~ 30 for both EMIC bands on occasion. Considerable wave power is present over a range f_m/f_{cHe} (panels c and d), with the distribution particularly heavy tailed for helium band EMIC waves (panel d). Again for comparison, f_m/f_{cHe} and the frequency cut-offs $(f_m \pm 2f_w)/f_{cHe}$ of the Gaussian spectra that are assumed by Kersten2014 are shown in blue. It is clear that the spectrum used by Kersten2014 does not overlap with the f_m/f_{cHe} of a substantial fraction of observations. Additionally, each of the EMIC observations has a finite spectral width, further increasing the wave power coverage to higher and lower ratios. Significant wave power is therefore present close to the bounding upper gyrofrequency, which may substantially affect electron diffusion. Finally, the central frequency and frequency range assumed by Ma et al. (2015) (henceforth Ma2015) and Drozdov et al. (2017) for He^+ EMIC waves is shown in Figure 1d. Their power spectrum lies within the tail of the distribution of fitted f_m/f_{cHe} with only $\sim 1\%$ exceeding their adopted value, suggesting their choice is unrepresentatively close to the helium ion gyrofrequency.

3. Diffusion Coefficients

In order to determine the effects of EMIC waves on radiation belt electrons, we calculate bounce-averaged diffusion coefficients for each observation using the concurrent spectral and plasma measurements (Watt et al., 2019). These results are then combined to create statistical bounce and drift-averaged diffusion coefficients. Although simulations suggest that EMIC waves can become highly nonlinear (Omura & Zhao, 2012), here we assume that the wave amplitude is sufficiently low and that the waves are sufficiently broad band

that quasi-linear theory can be applied. The concurrent measurement bounce-averaged diffusion coefficients for each CRRES observation are calculated using the code PADIE (Glauert & Horne, 2005). PADIE solves the cold plasma dispersion relation and so does not include warm plasma effects. We assume there is no EMIC wave power at absolute magnetic latitudes greater than 20° within $L^* = 5.5$ (Meredith et al., 2003). However, Allen et al. (2015) found EMIC wave at larger absolute latitudes. Those at larger absolute latitudes are mainly linearly polarized and therefore more likely to be oblique. We are assuming the main contribution to diffusion comes from lower latitudes. Hence, our diffusion coefficients are a conservative estimate rather than an over estimate.

For each observation, we perform latitudinally restricted bounce-averaged diffusion coefficient calculations using 10 latitude bins evenly spaced in absolute latitude between the equator and 20° . The wave power is assumed to be 0 outside the bin while the wave spectrum and plasma properties inside are determined from the local observation mapped to that bin latitude. These latitudinally restricted bounce-averaged diffusion coefficients are then summed to calculate the bounce-averaged diffusion coefficient for that observation. The procedure is explained in more detail below.

For a given observation, the local observed ratio f_{pe}/f_{ce} , and the fitted ratios f_m/f_{cHe} and f_w/f_{cHe} are mapped to other latitudes assuming a dipole magnetic field and constant cold plasma density along a magnetic field line. We also assume that f_m and f_w are constant as the waves propagate along the magnetic field lines from their source regions close to the magnetic equator. EMIC waves are thought to become more oblique as they propagate to higher latitudes from the equator (Anderson et al., 1992; Thorne & Horne, 1994); however, Ni et al. (2015) investigated the sensitivity of electron diffusion to EMIC wave normal angle and found that the main differences were at $\alpha_{eq} < 40^\circ$ and $E > 5$ MeV. Therefore, following Kersten et al. (2014) to allow a direct comparison, we assume that the waves have a Gaussian distribution in X , $X = \tan \psi$, where ψ is the wave normal angle, centered on $\psi = 0$ with a width $X_w = \tan 15^\circ$. The cutoff in X is taken to be $2X_w$. For the ion composition we assume abundances of $(H^+, He^+, O^+) = (0.94, 0.05, 0.01)$ (Kersten et al., 2014).

In a cold plasma, EMIC waves of band i will only exist for $f_{ci+1} < f < f_{ci}$. When such a wave propagates to higher latitudes, f/f_{ci} decreases and f may approach f_{ci+1} from above, where $i + 1$ is the next ion species in the series $\{H^+, He^+, O^+\}$. At which point the waves will become unguided and may reflect, refract or damp (Horne & Thorne, 1993, 1994) and so we assume they no longer take part in wave-particle interactions. Since the ion-ion hybrid frequency usually lies very close to the heavier ion cyclotron frequency we introduce the condition that $f > f_{ci+1}$ into the calculation. Similarly, at low latitudes, the high-frequency tail of the power spectrum may approach f_{ci} from below. These waves will be damped by warm plasma effects due to wave-particle interactions with substantial populations of warm particles. As we are working in the cold plasma framework, we must not include wave power at frequencies where this theory breaks down, that is, when the refractive index tends to infinity at the waves as the wave frequency approaches the gyrofrequency. We therefore add the constraint that $f/f_{ci} < 0.97$.

After summing over magnetic latitude to calculate a bounce-averaged diffusion coefficient for each observation, the results are then binned by activity and L^* to construct average values. In this calculation, the individual bounce-averaged diffusion coefficients are summed within each bin and divided by the total number of observations, including those with no EMIC activity, within that bin, in order to obtain the average diffusion experienced at a given time within this bin. This results in bounce- and drift-averaged EMIC diffusion coefficients for the given activity and L^* binning. For the L^* bins we use a step size of $0.5L^*$.

In Figures 2d–2f we show the resulting pitch angle diffusion coefficients for our K_p parametrization at L^* of 4, 4.5, and 5 during moderate activity, $2 \leq K_p < 4$. As expected, the diffusion is strongest at lower pitch angle and at higher energies but extends up to nearly 90° equatorial pitch angle, α_{eq} . Stronger diffusion is found at $L^* = 5$ as a result of more frequent EMIC wave activity. Electron diffusion by EMIC waves increases with K_p (not shown) but significant diffusion occurs even at relatively low K_p , Figures 2d–2f. This is in contrast to diffusion coefficients parametrized by P_{dyn} , Figures 2a–2c, where a much stronger activity dependence is found and there is significantly lower diffusion at $P_{dyn} < 5$ nPa, suggesting that electron scattering by EMIC waves is strongly influenced by P_{dyn} .

In the lowest two panels of Figure 2, we compare the new K_p parametrized coefficients against previous results obtained by Kersten2014 and Ma2015. Note that we have reproduced Ma2015's calculations with

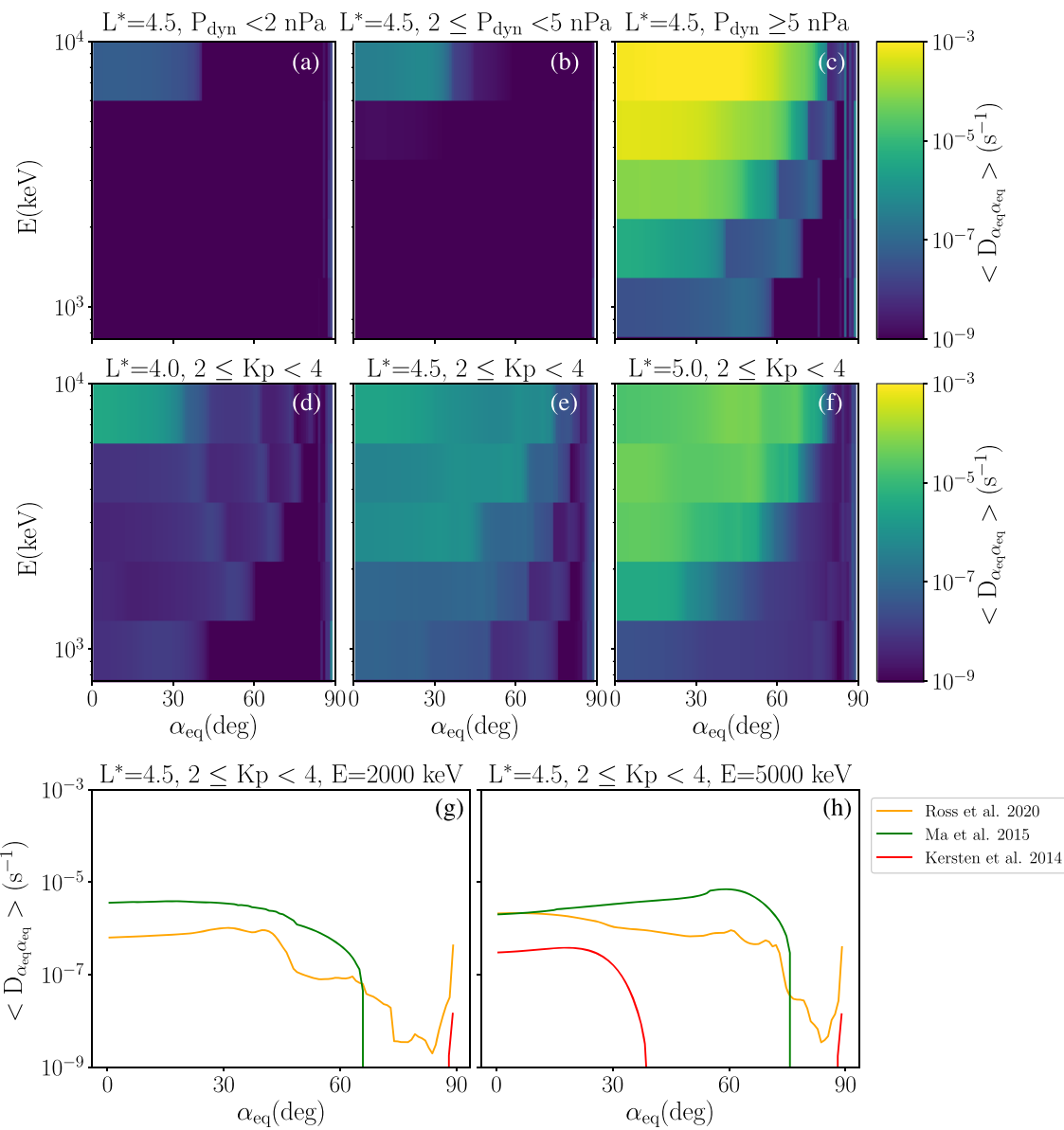


Figure 2. (a–c) The new EMIC wave bounce-averaged diffusion coefficients at $L^* = 5$ for $P_{dyn} < 2$, $2 \leq P_{dyn} < 5$, and $P_{dyn} \geq 5$ (nPa). Similarly, panels (d)–(f) show the diffusion coefficients at $L^* = 4$, 4.5, and 5 with $2 \leq K_p < 4$. Panels (g) and (h) show line plots of these diffusion coefficients in orange and, for comparison, the corresponding values from Kersten2014 (red) and from Ma2015 (green) are included.

$X = \tan(1^\circ)$ to approximate the field-aligned formalism. At 2 MeV (panel g), the Kersten et al. (2014) diffusion coefficients are largely 0, while Ma2015 show a higher level of diffusion to those calculated here, $\approx 10^{-6}$ (s) $^{-1}$, up to $\lesssim 65^\circ$ equatorial pitch angle. At higher pitch angles, our new diffusion coefficients provide a low-level diffusion, $\approx 10^{-8}$ s $^{-1}$, but there is no diffusion in Ma2015, this difference is due to the range of f_{pe}/f_{ce} captured in the new model. At 5 MeV (panel h), Ma2015 and the concurrent diffusion coefficients are both $\approx 10^{-6}$ s $^{-1}$ for $\alpha_{eq} \lesssim 30^\circ$, but by $\alpha_{eq} \lesssim 70^\circ$, Ma2015 exceed the concurrent diffusion coefficients by an order of magnitude. Again, our new diffusion coefficients provide low-level diffusion up to 90° equatorial pitch angle, however; Ma2015 give no diffusion for $\alpha_{eq} \gtrsim 75^\circ$. At this highly relativistic energy, Kersten et al. (2014) show diffusion only at pitch angles $\lesssim 40^\circ$.

4. Effects of EMIC Waves on Electron Fluxes

In the previous section we calculated diffusion coefficients for EMIC wave-particle interactions using concurrent measurements. We will now assess their implications on radiation belt electron modeling. For this

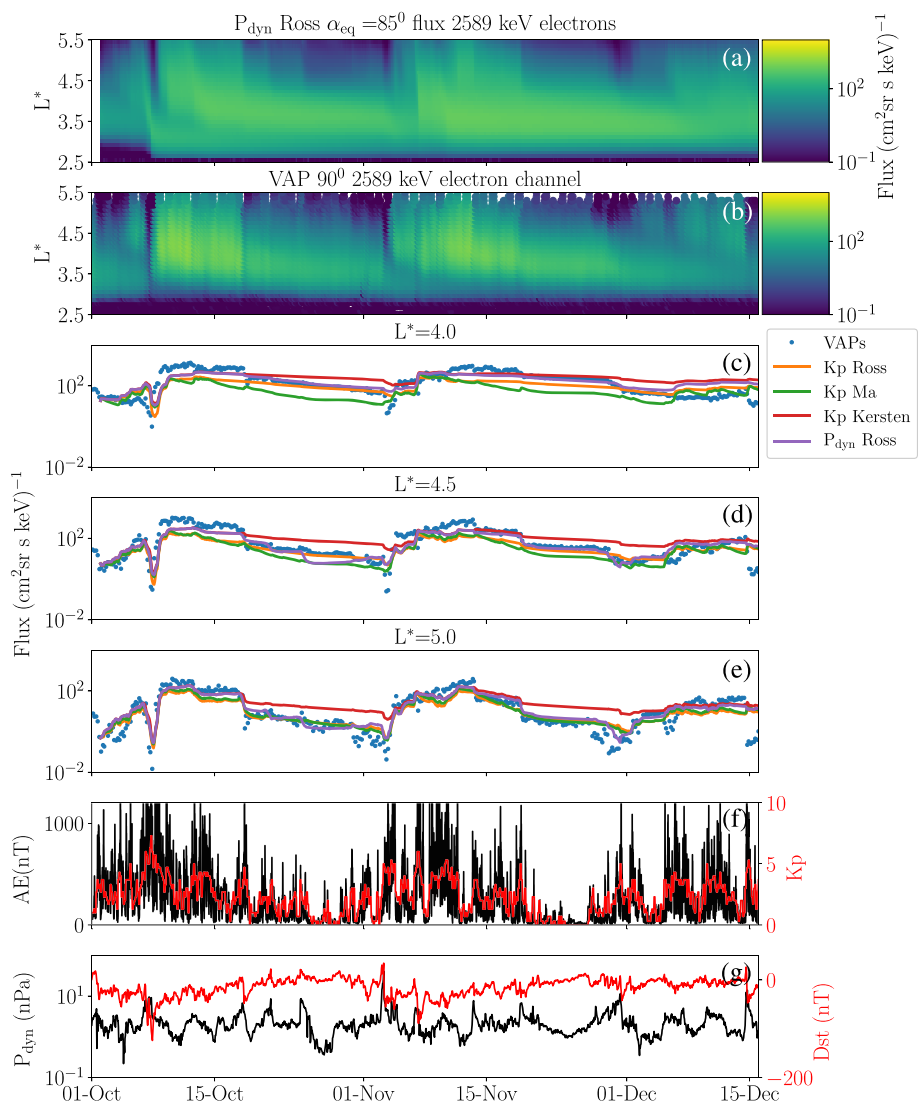


Figure 3. Comparison between 2.589 MeV electron flux observed by the Van Allen Probes and the flux simulated by BAS-RBM during the period 2 October to 15 November 2015. Panel (a) shows the radial profile of the 2.589 MeV electron flux from BAS-RBM, and panel (b) show the flux observed by the Van Allen Probes. Panels (c) and (d) again show the 2.589 MeV flux at $L^* = 4.0, 4.5, 5.0$, respectively. The blue dots show the observed flux and the colored lines are the simulated values. Panel (e) and (f) show AE , Kp , P_{dyn} , and Dst .

study, we perform 3-D simulations of the Earth's radiation belts using the British Antarctic Survey Radiation Belt Model (BAS-RBM) (Glauert et al., 2014a, 2014b), which is based on the phase-averaged Fokker-Plank equation that calculates the evolution of the electron phase space density. Primarily, BAS-RBM simulations are used for reproducing historical events and short-term forecasting. Currently, Kp is forecasted and used as a wave parametrization index when observational data is unavailable. In addition to Kp with bin infima of {0, 2, 4, 6} (henceforth Kp Ross), we present results using solar wind pressure, P_{dyn} , as the EMIC driving index (henceforth P_{dyn} Ross) with bin infima of {0, 2, 5} nPa. This choice is motivated by the observed link between solar wind pressure and EMIC activity (Anderson & Hamilton, 1993; Lessard et al., 2019; Saikin et al., 2016; Usanova et al., 2012). Additionally, Drozdov et al. (2017) found that a P_{dyn} EMIC wave parametrization minimized the mean absolute error of 4.2 MeV electrons in radiation belt simulations. For comparison, we also present two otherwise identical simulations where the EMIC waves are from Kersten et al. (2014) and Ma et al. (2015), parametrized by Kp (henceforth Kp Kersten and Kp Ma).

For these runs, we consider the time period 2 October to 15 December 2015. Van Allen Probes background corrected MagEIS electron fluxes (Blake et al., 2013; Claudepierre et al., 2015), and REPT (Baker et al., 2013)

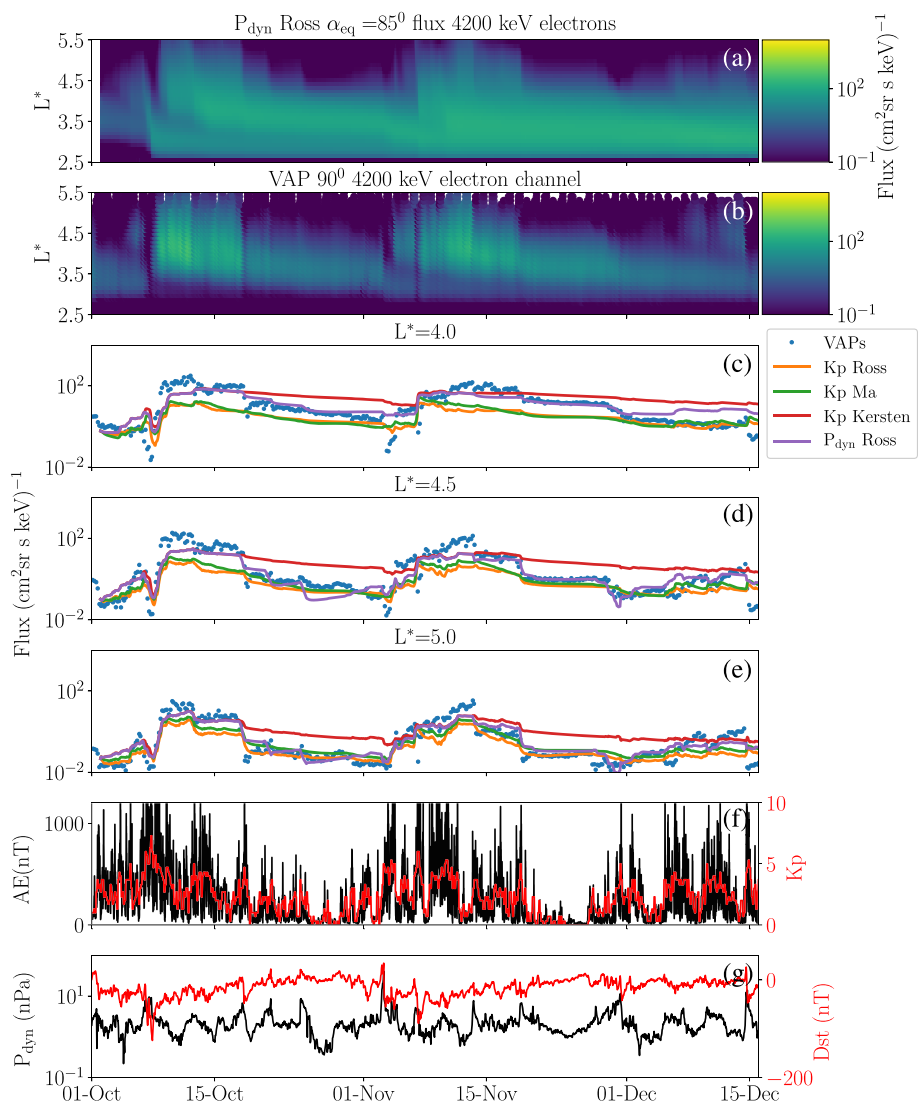


Figure 4. The same as Figure 3 but for 4.2 MeV electrons.

electron fluxes are used for both the initial condition and the boundary conditions at L_{min} , L_{max} , and E_{min} . The inner L^* boundary is set to 2.5 and the outer L^* boundary to 5.5. The minimum energy boundary is determined by assuming constant first adiabatic invariant with $E = 150$ keV at the outer L^* boundary. Note that BAS-RBM assumes a dipole magnetic field configuration and so $L^* = L$, although the wave measurements are converted to L^* (section 2). The chorus diffusion coefficients are parametrized by AE (Horne et al., 2013), and the hiss diffusion coefficients are also parametrized by AE (Meredith et al., 2018). The chorus and hiss waves are spatially separated by an activity dependent mask as given in Meredith et al. (2018). For radial diffusion we use the Kp -driven magnetic component of the (Brautigam & Albert, 2000) formalism. The location of the last closed drift shell is accounted for following Glauert et al. (2014a).

In Figure 3 we show the results of our simulations at 2.6 MeV. In panel (e) we compare the $\alpha_{eq} = 85^\circ$ simulated flux at $L^* = 5$ to Van Allen Probe data. P_{dyn} Ross (purple), Kp Ross (orange), and Kp Ma (green) significantly improve the agreement between the modeled and observed (blue) 2.6 MeV equatorially mirroring electron fluxes compared to Kp Kersten (red). This is most apparent during quasi-steadily decaying times and during rapid loss. For instance, in mid-October 2015, a rapid order of magnitude decease occurs followed by ~ 10 days of steady decay. P_{dyn} Ross, Kp Ross, and Kp Ma reproduce the rapid drop and slow decay; however, the losses during both of these phases is insufficient in Kp Kersten, leading to approximately an order of magnitude discrepancy between modeled and observed fluxes by the 1 November. At lower L^* ,

panels (c) and (d), P_{dyn} Ross and Kp Ross again perform better than Kp Kersten, with decay consistent with observations. Contrastingly, Kp Ma underestimates the electron fluxes at $L^* = 4$. During electron acceleration phases, such as early October and early November, the flux in Kp Ross and Kp Ma are a factor of ~ 2 less than is obtained in the P_{dyn} Ross and Kp Kersten, leading to a greater discrepancy with observations. This is due to additional losses in this run coincident with the acceleration as a result of large Kp , as seen in panel (f). Note that Kp Ma has constant EMIC activity above $Kp = 2$. From panels (a) and (b), it is clear that the agreement at $L^* < 4$ between the models and the observations is significantly worse than at $L^* \gtrsim 4.0$. In particular, relativistic electrons are transported into the slot region in the simulation, while this is not found in the observational data. This is likely a result of a combination of factors. First, our EMIC diffusion coefficients do not extend below $L^* = 3.5$ due to lack of EMIC observations in the CRRES data set as a result of the magnetometer switched into low sensitivity mode in this region and EMIC waves were unable to be identified at these times. At $L^* < 4.0$ the CRRES observational coverage is unlikely to be sufficient to calculate reliable diffusion coefficients in this way. Contrastingly, the statistical coverage of EMIC waves peaks at $L^* \sim 5$ where the discrepancy between modeled fluxes and observations is at its minimum (Meredith et al., 2014). Second, rapid injection of electrons via radial transport is not always well captured by a simple radial diffusion parametrization.

Figure 4 is equivalent to Figure 3 but for 4.2 MeV electrons. At $L^* = 5.0$, panel (e), P_{dyn} Ross, Kp Ross, and Kp Ma give better agreement with observed fluxes than Kp Kersten. In particular, Kp Kersten does not reproduce the magnitude of the rapid decreases in flux that occur. At $L^* = 4.5$, P_{dyn} Ross agrees more closely with observations than the other three models, with Kp Ma performing better than Kp Ross and Kp Kersten. As was the case at 2.6 MeV, Kp Ross and Kp Ma significantly underestimate the local maxima in 4.2 MeV electron flux but reproduce the temporal evolution at lower fluxes. Again this is indicative of excessive loss during enhanced Kp while acceleration is occurring. P_{dyn} , on the other hand, only provides short-lived pulses of EMIC diffusion, while $P_{dyn} > 5$ nPa (see Figures 2a–2c), which coincides with observed rapid flux depletions, allowing high-energy electron fluxes to increase relatively unimpeded. Contrastingly, Kp Kersten exhibits minimal diffusion of equatorially mirroring particles even during enhanced Kp , resulting in consistent underestimation of losses. The behavior at $L^* = 4.0$, of the four runs is similar to that at $L^* = 4.5$. The most notable difference being a significantly larger discrepancy between observed fluxes and those in P_{dyn} Ross. This again suggests that the observational coverage EMIC coverage of CRRES is insufficient, at $L^* \lesssim 4$, to fully reproduce relativistic electron decay.

5. Discussion

In this paper we have presented a new approach for calculating, using quasi-linear theory, average diffusion coefficients representing the diffusion of electrons by EMIC waves by averaging over observation-specific diffusion coefficients. In our EMIC diffusion model, we are assuming that electrons interact with EMIC waves sufficiently frequently on the diffusion timescale for an average representation to be appropriate. We have shown that 3-D Fokker-Planck radiation belt models using these new concurrent measurement EMIC diffusion coefficients considerably improve agreement between modeled and observed decay of relativistic electrons in the outer radiation belt at $L^* \gtrsim 4$ when compared to models using EMIC diffusion coefficients calculated from average spectral and plasma properties, with the strongest agreement when the EMIC diffusion coefficients are parametrized by P_{dyn} . In particular, relativistic near-equatorially mirroring electrons are scattered in pitch angle by the EMIC waves and are eventually precipitated into the atmosphere. This is in contrast to equivalent simulations using EMIC diffusion coefficients constructed using averaged spectral and plasma properties. It is necessary to capture the effects of the full range of wave-particle interactions that occur, not only those of an interaction under average conditions and with average spectral properties. Diffusion is possible over a wider domain in (α_{eq}, E, L^*) space than is otherwise found using the simpler prescription. More precisely, diffusion extends nearly to 90° and so electron losses into the atmosphere are possible over a much wider range of pitch angles than before. The differing behavior is a result of the wave-particle interactions in high-density regions and when the wave frequency is close to the EMIC wave bands upper gyrofrequency. At $E = 4.2$ MeV, the results of our Kp driven model are comparable to a Kp -driven model using an EMIC spectral profile where the central wave frequency is chosen to be close to the upper-bounding gyrofrequency following Ma et al. (2015). Contrastingly, at $E = 2.6$ MeV, our Kp -driven

EMIC model gives closer agreement to observations at $L^* = 4.0$. Our analysis of CRRES EMIC observations suggest that the central spectral frequency to helium gyrofrequency adopted in Ma et al. (2015) is unrepresentatively high and is only reached or exceeded in $\sim 1\%$ of EMIC observations.

The L^* range of the EMIC diffusion coefficients calculated here is limited due to the CRRES 16 Hz magnetometer data set having no identifiable EMIC observations at $L^* \lesssim 3.5$. Contrastingly, Qin et al. (2019) found EMIC waves at L^* as low as ~ 2.5 using the 64 Hz fluxgate magnetometer, EMFISIS, on board the Van Allen Probes. Additionally, owing to the brevity of the CRRES mission and the infrequency of EMIC waves, the statistical coverage of $L^* \lesssim 4$ is insufficient to create representative diffusion coefficients from the limited number of measurements. New Van Allen Probe observations of EMIC waves down to $L^* \sim 2.5$, and thus, the method shown here may help reduce the uncertainty in modeling the decay of the ultrarelativistic storage ring (Baker et al., 2013; Shprits et al., 2016; Usanova et al., 2014).

Given the improvement in the global simulations found when using our new diffusion coefficients, we propose that a similar approach should be explored for hiss and chorus waves as suggested in Watt et al. (2019). In this way plasma density and wave spectral variation will be included implicitly and thus enable a much better calculation of electron acceleration to relativistic energies which becomes very effective in low-density regions.

Data Availability Statement

The authors used geomagnetic indices provided by OMNIWeb ([Phttps://omniweb.gsfc.nasa.gov](https://omniweb.gsfc.nasa.gov)), the Van Allen Probes data (<http://www.rbsp-ect.lanl.gov/>), and the IRBEM library (<https://craterre.onera.fr/prbem/irbem/description.html>). The results shown in this paper can be downloaded from the U.K. Polar Data Centre (at <https://doi.org/10.5285/be8af49f-cdf1-443a-9c78-6a59c9d5be68>).

Acknowledgments

The research leading to these results has received funding from the National Environment Research Council Highlight Topic grants NE/P01738X/1 and NE/P017274/1, National Environment Research Council grants NE/R016445/1 and NE/R016038/1, and the STFC grants ST/S000496/1 and ST/R000921/1. The authors would like to thank Brian Fraser for providing the CRRES EMIC wave data set.

References

- Albert, J. M. (2003). Evaluation of quasi-linear diffusion coefficients for EMIC waves in a multispecies plasma. *Journal of Geophysical Research*, 108(A6), 1249. <https://doi.org/10.1029/2002JA009792>
- Allen, R. C., Zhang, J.-C., Kistler, L. M., Spence, H. E., Lin, R.-L., Klecker, B., et al. (2015). A statistical study of EMIC waves observed by Cluster: 1. Wave properties. *Journal of Geophysical Research: Space Physics*, 120, 5574–5592. <https://doi.org/10.1002/2015JA021333>
- Anderson, B. J., Erlandson, R. E., & Zanetti, L. J. (1992). A statistical study of Pc 1-2 magnetic pulsations in the equatorial magnetosphere: 2. Wave properties. *Journal of Geophysical Research*, 97(A3), 3089–3101. <https://doi.org/10.1029/91ja02697>
- Anderson, B. J., & Hamilton, D. C. (1993). Electromagnetic ion cyclotron waves stimulated by modest magnetospheric compressions. *Journal of Geophysical Research*, 98(A7), 11369. <https://doi.org/10.1029/93ja00605>
- Baker, D. N., Blake, J. B., Callis, L. B., Cummings, J. R., Hovestadt, D., Kanekal, S., et al. (1994). Relativistic electron acceleration and decay time scales in the inner and outer radiation belts: SAMPEX. *Geophysical Research Letters*, 21(6), 409–412. <https://doi.org/10.1029/93GL03532>
- Baker, D. N., Kanekal, S. G., Hoxie, V. C., Henderson, M. G., Li, X., Spence, H. E., et al. (2013). A long-lived relativistic electron storage ring embedded in Earth's outer Van Allen Belt. *Science*, 340(6129), 186–190. <https://doi.org/10.1126/science.1233518>
- Blake, J. B., Carranza, P. A., Claudepierre, S. G., Clemmons, J. H., Crain, W. R., Dotan, Y., et al. (2013). The Magnetic Electron Ion Spectrometer (MagEIS) instruments aboard the Radiation Belt Storm Probes (RBSP) spacecraft. *Space Science Reviews*, 179(1–4), 383–421. <https://doi.org/10.1007/s11214-013-9991-8>
- Blake, J. B., Kolasinski, W. A., Fillius, R. W., & Mullen, E. G. (1992). Injection of electrons and protons with energies of tens of MeV into L < 3 on 24 March 1991. *Geophysical Research Letters*, 19(8), 821–824. <https://doi.org/10.1029/92GL00624>
- Brautigam, D. H., & Albert, J. M. (2000). Radial diffusion analysis of outer radiation belt electrons during the October 9, 1990, magnetic storm. *Journal of Geophysical Research*, 105(A1), 291–309. <https://doi.org/10.1029/1999JA900344>
- Claudepierre, S. G., Ma, Q., Bortnik, J., O'Brien, T. P., Fennell, J. F., & Blake, J. B. (2020). Empirically estimated electron lifetimes in the Earth's radiation belts: Van Allen Probe observations. *Geophysical Research Letters*, 47, e2019GL086053. <https://doi.org/10.1029/2019GL086053>
- Claudepierre, S. G., O'Brien, T. P., Blake, J. B., Fennell, J. F., Roeder, J. L., Clemmons, J. H., et al. (2015). A background correction algorithm for Van Allen Probes MagEIS electron flux measurements. *Journal of Geophysical Research: Space Physics*, 120, 5703–5727. <https://doi.org/10.1002/2015JA021171>
- Drozdov, A. Y., Shprits, Y. Y., Usanova, M. E., Aseev, N. A., Kellerman, A. C., & Zhu, H. (2017). EMIC wave parameterization in the long-term VERB code simulation. *Journal of Geophysical Research: Space Physics*, 122, 8488–8501. <https://doi.org/10.1002/2017JA024389>
- Glauert, S. A., & Horne, R. B. (2005). Calculation of pitch angle and energy diffusion coefficients with the PADIE code. *Journal of Geophysical Research*, 110, A04206. <https://doi.org/10.1029/2004JA010851>
- Glauert, S. A., Horne, R. B., & Meredith, N. P. (2014a). Simulating the Earth's radiation belts: Internal acceleration and continuous losses to the magnetopause. *Journal of Geophysical Research: Space Physics*, 119, 7444–7463. <https://doi.org/10.1002/2014JA020092>
- Glauert, S. A., Horne, R. B., & Meredith, N. P. (2014b). Three-dimensional electron radiation belt simulations using the BAS Radiation Belt Model with new diffusion models for chorus, plasmaspheric hiss, and lightning-generated whistlers. *Journal of Geophysical Research: Space Physics*, 119, 268–289. <https://doi.org/10.1002/2013JA019281>
- Horne, R. B., Kersten, T., Glauert, S. A., Meredith, N. P., Boscher, D., Sicard-Piet, A., et al. (2013). A new diffusion matrix for whistler mode chorus waves. *Journal of Geophysical Research: Space Physics*, 118, 6302–6318. <https://doi.org/10.1002/jgra.50594>

- Horne, R. B., & Thorne, R. M. (1993). On the preferred source location for the convective amplification of ion cyclotron waves. *Journal of Geophysical Research*, 98(A6), 9233–9247. <https://doi.org/10.1029/92JA02972>
- Horne, R. B., & Thorne, R. M. (1994). Convective instabilities of electromagnetic ion cyclotron waves in the outer magnetosphere. *Journal of Geophysical Research*, 99(A9), 17,259–17,273. <https://doi.org/10.1029/94JA01259>
- Horne, R. B., & Thorne, R. M. (1998). Potential waves for relativistic electron scattering and stochastic acceleration during magnetic storms. *Geophysical Research Letters*, 25(15), 3011–3014. <https://doi.org/10.1029/98GL01002>
- Horne, R. B., Thorne, R. M., Glauert, S. A., Albert, J. M., Meredith, N. P., & Anderson, R. R. (2005). Timescale for radiation belt electron acceleration by whistler mode chorus waves. *Journal of Geophysical Research*, 110, A03225. <https://doi.org/10.1029/2004JA010811>
- Horne, R. B., Thorne, R. M., Shprits, Y. Y., Meredith, N. P., Glauert, S. A., Smith, A. J., et al. (2005). Wave acceleration of electrons in the Van Allen radiation belts. *Nature*, 437(7056), 227–230. <https://doi.org/10.1038/nature03939>
- Johnson, M. H., & Kierlein, J. (1992). Combined Release and Radiation Effects Satellite (CRRES): Spacecraft and mission. *Journal of Spacecraft and Rockets*, 29(4), 556–563. <https://doi.org/10.2514/3.55641>
- Kersten, T., Horne, R. B., Glauert, S. A., Meredith, N. P., Fraser, B. J., & Grew, R. S. (2014). Electron losses from the radiation belts caused by EMIC waves. *Journal of Geophysical Research: Space Physics*, 119, 8820–8837. <https://doi.org/10.1002/2014JA020366>
- Lessard, M. R., Paulson, K., Spence, H. E., Weaver, C., Engebretson, M. J., Millan, R., et al. (2019). Generation of EMIC waves and effects on particle precipitation during a solar wind pressure intensification with $Bz > 0$. *Journal of Geophysical Research: Space Physics*, 124, 4492–4508. <https://doi.org/10.1029/2019JA026477>
- Ma, Q., Li, W., Thorne, R. M., Ni, B., Kletzing, C. A., Kurth, W. S., et al. (2015). Modeling inward diffusion and slow decay of energetic electrons in the Earth's outer radiation belt. *Geophysical Research Letters*, 42, 987–995. <https://doi.org/10.1002/2014GL062977>
- Meredith, N. P., Horne, R. B., Clilverd, M. A., Horsfall, D., Thorne, R. M., & Anderson, R. R. (2006). Origins of plasmaspheric hiss. *Journal of Geophysical Research*, 111, A09217. <https://doi.org/10.1029/2006JA011707>
- Meredith, N. P., Horne, R. B., Kersten, T., Fraser, B. J., & Grew, R. S. (2014). Global morphology and spectral properties of EMIC waves derived from CRRES observations. *Journal of Geophysical Research: Space Physics*, 119, 5328–5342. <https://doi.org/10.1002/2014JA020064>
- Meredith, N. P., Horne, R. B., Kersten, T., Li, W., Bortnik, J., Sicard, A., & Yearby, K. H. (2018). Global model of plasmaspheric hiss from multiple satellite observations. *Journal of Geophysical Research: Space Physics*, 123, 4526–4541. <https://doi.org/10.1029/2018JA025226>
- Meredith, N. P., Horne, R. B., Summers, D., Thorne, R. M., Iles, R. H. A., Heynderickx, D., & Anderson, R. R. (2002). Evidence for acceleration outer zone electrons to relativistic energies by whistler mode chorus. *Annales Geophysicae*, 20(7), 967–979. <https://doi.org/10.5194/angeo-20-967-2002>
- Meredith, N. P., Thorne, R. M., Horne, R. B., Summers, D., Fraser, B. J., & Anderson, R. R. (2003). Statistical analysis of relativistic electron energies for cyclotron resonance with EMIC waves observed on CRRES. *Journal of Geophysical Research*, 108(A6), 1250. <https://doi.org/10.1029/2002JA009700>
- Miyoshi, Y., Sakaguchi, K., Shiokawa, K., Evans, D., Albert, J., Connors, M., & Jordanova, V. (2008). Precipitation of radiation belt electrons by EMIC waves, observed from ground and space. *Geophysical Research Letters*, 35, L23101. <https://doi.org/10.1029/2008GL035727>
- Ni, B., Cao, X., Zou, Z., Zhou, C., Gu, X., Bortnik, J., et al. (2015). Resonant scattering of outer zone relativistic electrons by multiband EMIC waves and resultant electron loss time scales. *Journal of Geophysical Research: Space Physics*, 120, 7357–7373. <https://doi.org/10.1002/2015JA021466>
- Olson, W. P., & Pfitzer, K. A. (1977). Magnetospheric magnetic field modeling. Annual scientific report. Air Force Office of Sci. Res.
- Omura, Y., & Zhao, Q. (2012). Nonlinear pitch angle scattering of relativistic electrons by EMIC waves in the inner magnetosphere. *Journal of Geophysical Research*, 117, A08227. <https://doi.org/10.1029/2012JA017943>
- Qin, M., Hudson, M., Li, Z., Millan, R., Shen, X., Shprits, Y., et al. (2019). Investigating loss of relativistic electrons associated with EMIC waves at low L values on 22 June 2015. *Journal of Geophysical Research: Space Physics*, 124, 4022–4036. <https://doi.org/10.1029/2018JA025726>
- Reeves, G. D., McAdams, K. L., Friedel, R. H. W., & O'Brien, T. P. (2003). Acceleration and loss of relativistic electrons during geomagnetic storms. *Geophysical Research Letters*, 30(10), 1529. <https://doi.org/10.1029/2002gl016513>
- Rodger, C. J., Raita, T., Clilverd, M. A., Seppälä, A., Dietrich, S., Thomson, N. R., & Ulich, T. (2008). Observations of relativistic electron precipitation from the radiation belts driven by EMIC waves. *Geophysical Research Letters*, 35, L16106. <https://doi.org/10.1029/2008GL034804>
- Saikin, A. A., Zhang, J. C., Smith, C. W., Spence, H. E., Torbert, R. B., & Kletzing, C. A. (2016). The dependence on geomagnetic conditions and solar wind dynamic pressure of the spatial distributions of EMIC waves observed by the Van Allen Probes. *Journal of Geophysical Research A: Space Physics*, 121, 4362–4377. <https://doi.org/10.1002/2016JA022523>
- Schulz, M., & Lanzerotti, L. J. (1974). *Particle diffusion in the radiation belts*. New York: Springer. <https://doi.org/10.1007/978-3-642-65675-0>
- Shprits, Y. Y., Drozdov, A. Y., Spasojevic, M., Kellerman, A. C., Usanova, M. E., Engebretson, M. J., et al. (2016). Wave-induced loss of ultra-relativistic electrons in the Van Allen radiation belts. *Nature Communications*, 7, 1–7. <https://doi.org/10.1038/ncomms12883>
- Shprits, Y. Y., Kellerman, A., Aseev, N., Drozdov, A. Y., & Michaelis, I. (2017). Multi-MeV electron loss in the heart of the radiation belts. *Geophysical Research Letters*, 44, 1204–1209. <https://doi.org/10.1002/2016GL072258>
- Singer, H. J., Sullivan, W. P., Anderson, P., Mozer, F., Harvey, P., Wygant, J., & McNeil, W. (1992). Fluxgate magnetometer instrument on the CRRES. *Journal of Spacecraft and Rockets*, 29(4), 599–601. <https://doi.org/10.2514/3.25506>
- Summers, D., Ni, B., & Meredith, N. P. (2007). Timescales for radiation belt electron acceleration and loss due to resonant wave-particle interactions: 2. Evaluation for VLF chorus, ELF hiss, and electromagnetic ion cyclotron waves. *Journal of Geophysical Research*, 112, A04207. <https://doi.org/10.1029/2006JA011993>
- Thorne, R. M., & Horne, R. B. (1994). Energy transfer between energetic ring current H^+ and O^+ by electromagnetic ion cyclotron waves. *Journal of Geophysical Research*, 99(A9), 17,275–17,282. <https://doi.org/10.1029/94JA01007>
- Ukhorskiy, A. Y., Shprits, Y. Y., Anderson, B. J., Takahashi, K., & Thorne, R. M. (2010). Rapid scattering of radiation belt electrons by storm-time EMIC waves. *Geophysical Research Letters*, 37, L09101. <https://doi.org/10.1029/2010GL042906>
- Usanova, M. E., Drozdov, A., Orlova, K., Mann, I. R., Shprits, Y., Robertson, M. T., et al. (2014). Effect of EMIC waves on relativistic and ultrarelativistic electron populations: Ground-based and Van Allen Probes observations. *Geophysical Research Letters*, 41, 1375–1381. <https://doi.org/10.1002/2013GL059024>
- Usanova, M. E., Mann, I. R., Bortnik, J., Shao, L., & Angelopoulos, V. (2012). THEMIS observations of electromagnetic ion cyclotron wave occurrence: Dependence on AE, SYMH, and solar wind dynamic pressure. *Journal of Geophysical Research*, 117, A10218. <https://doi.org/10.1029/2012JA018049>

- Watt, C. E. J., Allison, H. J., Meredith, N. P., Thompson, R. L., Bentley, S. N., Rae, I. J., et al. (2019). Variability of quasilinear diffusion coefficients for plasmaspheric hiss. *Journal of Geophysical Research: Space Physics*, 124, 8488–8506. <https://doi.org/10.1029/2018JA026401>
- Wrenn, G. L., Rodgers, D. J., & Ryden, K. A. (2002). A solar cycle of spacecraft anomalies due to internal charging. *Annales Geophysicae*, 20(7), 953–956. <https://doi.org/10.5194/angeo-20-953-2002>
- Yuan, Z., Liu, K., Yu, X., Yao, F., Huang, S., Wang, D., & Ouyang, Z. (2018). Precipitation of radiation belt electrons by EMIC waves with conjugated observations of NOAA and Van Allen satellites. *Geophysical Research Letters*, 45, 12,694–12,702. <https://doi.org/10.1029/2018GL080481>